Multiscale Modeling of High Velocity Impact Damage on Composite Structures

I. Smojver and D. Ivančević

Department of Aeronautical Engineering, Faculty of Mechanical Engineering and Naval Architecture, University of Zagreb

I. Lučića 5, HR-10000, Zagreb, Croatia

Abstract: *A multiscale damage prediction procedure has been developed which employs Abaqus/Explicit to solve the problem at the structural level of composite structures. The multiscale framework has been established applying the user material subroutine VUMAT which is coupled with the micromechanical model. The procedure is based on a computationally enhanced version of the High Fidelity Generalized Method of Cells (HFGMC) micromechanical model. The two-scale approach enables calculation of the stress field within the unit cell, based on the constitutive behavior of each subcell and the unit cell morphology. As the stress distribution is determined for the representative unit cells, calculations of failure criteria and damage effects in the composite are performed at the micro-level. Failure initiation has been predicted using three micromechanical failure criteria – the 3D Tsai-Hill model, the MultiContinuum Theory model and the 3D Hashin strain based failure criteria. The procedure is intended to establish a multiscale framework for modeling of high velocity impact damage processes at aeronautical composite structures (e.g. birdstrike, hail impact, etc.). The procedure has been tested on a numerical example in which a soft body impactor impacts a CFRP plate. The Coupled Eulerian Lagrangian formulation has been employed for modeling of the highly deformable impactor, while EOS material models have been used for soft body constitutive models.*

Keywords: *High Fidelity Generalized Method of Cells, Multiscale analysis, Composite materials, Abaqus/Explicit, High velocity impact.*

List of the most important symbols:

$\mathbf{A}^{(\beta,\gamma)}$ - strain concentration tensor of the β,γ subcell

$\mathbf{C}^{(\beta,\gamma)}$ - elasticity tensor of the β,γ subcell

$\mathbf{C}^{*}$ - equivalent elasticity tensor

h_β, l_γ - subcell dimensions in *2* and *3* directions, respectively

N_β, N_γ - number of subcells in *2* and *3* directions, respectively

V_f - fiber volume fraction

$u_i^{(\beta,\gamma)}$ - displacement field approximation of the β,γ subcell

$W_{i(mn)}^{(\beta,\gamma)}$ - microvariables of the β,γ subcell

$\overline{\boldsymbol{\varepsilon}}^{(\beta,\gamma)}$ - strain tensor of the β,γ subcell

$\overline{\boldsymbol{\varepsilon}}$ - macroscopic strain tensor

ε_i^D - damage strains

$\overline{\boldsymbol{\sigma}}^{(\beta,\gamma)}$ - stress tensor of the β,γ *subcell*

1. Introduction

The simulation of bird strike induced damage in composite structures is a numerically challenging task in which several physical phenomena have to be accurately modeled in order to obtain reliable results. The numerical challenges include modeling of extremely high deformations of the impactor and complex contact conditions between the impacting material and the impacted structure. An important part of the numerical methodology is correct modeling of the forces which are imposed on the impacted structure during the simulated event. These forces depend on the substitute bird mechanical properties and the employed contact algorithm. Finally, the numerical model of the impacted structure has to be able to simulate complex failure modes of laminated composite structures.

The bird strike is placed in the group of soft-body impacts, since the stresses generated in the impacting body greatly exceed the strength of the bird material. Consequently, the strength of the impacting material is neglected in numerical simulations and Equation of State (EOS) material models are usually employed to define constitutive behavior of the bird material. The methodology described in this work is a continuation of the work presented in (Ivančević, 2011, Smojver, 2011 and Smojver, 2012). Abaqus/Explicit has in the previous work been utilized within a bird strike damage prediction procedure which has been employed on complex aeronautical structures. An important feature of the methodology is the application of the Coupled Eulerian-Lagrangian (CEL) technique to capture the extreme deformations of the soft-body impactor. As demonstrated in (Smojver, 2012), the application of the CEL impactor resulted in significant improvements of the stability and accuracy of the methodology.

This work focuses on the damage and failure modeling of composite structures during the high velocity impact event.

As demonstrated in the World Wide Failure Exercise (*WWFE*), failure and damage modeling of composite materials is a very complex task. The comparison of several different failure theories resulted in large discrepancies of the predicted failure load, even for the simple static load cases. The problem becomes even more obvious for composite layups which include differently oriented composite plies (Hinton, 2004) and more complex loading conditions.

A contemporary approach to the problem of failure analysis of structures which are made of heterogeneous materials is the application of multiscale methods. Failure and damage have in these approaches been modeled using micromechanical principles, while application of the multiscale technique enables the usage of micromechanical theories on engineering problems. The multiscale framework has in the presented methodology been achieved using Abaqus/Explicit for structural-level computations, while the semi-analytical High Fidelity Generalized Method of Cells (HFGMC) has been employed as the micromechanical model (Aboudi, 2012). The described methodology is in the development phase, with several approaches to damage modeling currently being evaluated.

2. High Fidelity Generalized Method of Cells

The main objective of micromechanical models in the multiscale environment is prediction of homogenized mechanical properties of the heterogeneous material. Furthermore, micromechanical models enable calculation of strain and stress fields within the microstructure which is loaded by the macroscopic loading.

The HFGMC model belongs to the group of micromechanical models which have been developed from the Method of Cells (MOC) (Aboudi 1987). These micromechanical models are based on the Representative Unit Cell (RUC) concept, in which periodicity conditions are employed on the boundaries of the unit cell. The unit cell is a characteristic element of the evaluated heterogeneous material and therefore defines the macroscopic properties of the material. The discretization scheme and basic parameters of the HFGMC model are shown in Figure 1. A common feature of MOC-based micromechanical models is the discretization of the unit cell using $N_\beta \times N_\gamma$ rectangular subcells. The reformulated HFGMC, which has been employed in this work, introduces a computationally enhanced implementation of the governing HFGMC equations based on a local/global stiffness matrix approach (Bansal, 2006). A result of this computational approach is the improvement of computational efficiency by 60% compared to the original implementation (Bansal, 2005).

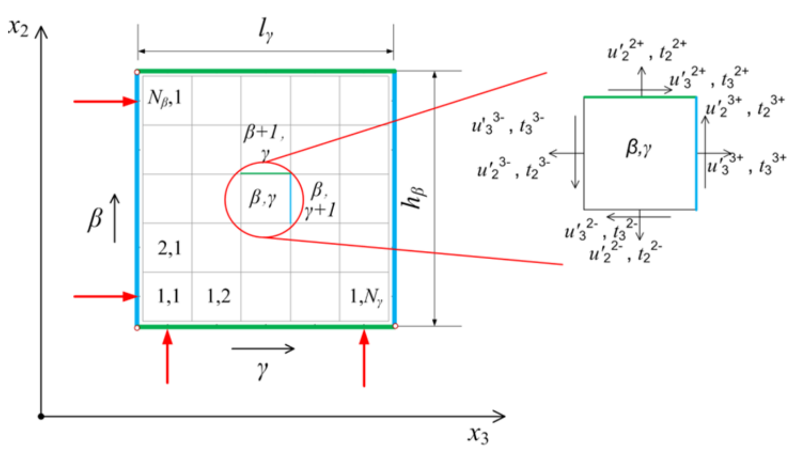

Figure 1. HFGMC micromechanical model.

Due to the complexity of the HFGMC model, only the basic outlines of the theory are provided in this work, while more details can be found in the references e.g. (Aboudi, 2003, Aboudi 2012). The micromechanical model is based on the second-order Legendre polynomial which is used to approximate the displacement field within the subcells, after (Aboudi, 2003).

$$u_i^{(\beta,\gamma)} = \bar{\varepsilon}_{ij} x_j + W_{i(00)}^{(\beta,\gamma)} + \bar{y}_2^{(\beta)} W_{i(10)}^{(\beta,\gamma)} + \bar{y}_3^{(\gamma)} W_{i(01)}^{(\beta,\gamma)} + \frac{1}{2}\left(3\bar{y}_2^{(\beta)2} - \frac{h_\beta^2}{4}\right) W_{i(20)}^{(\beta,\gamma)} + \\ + \frac{1}{2}\left(3\bar{y}_3^{(\gamma)2} - \frac{l_\gamma^2}{4}\right) W_{i(02)}^{(\beta,\gamma)} \quad i,j = 1,2,3. \tag{1}$$

The first term in Equation 1 is the contribution of the macroscopic strain $\bar{\varepsilon}_{ij}$ which is applied on the unit cell, while the other terms represent the fluctuating displacement field which has to be determined from the HFGMC solution. The solution of the micromechanical system of equations starts by the construction of subcell local stiffness matrices based on the subcell mechanical properties and dimensions. The stiffness matrices are merged into the global system of equations by application of displacement and traction continuity conditions between the subcells, and periodicity conditions in the global x_2 and x_3 directions on the unit cell boundaries. Additionally, four displacement components are constrained in order to prevent unit cell rigid body motion as displayed by the four arrows at the unit cell borders in Figure 1. The solution of the global system of equations enables calculation of the strain concentration tensor $\mathbf{A}^{(\beta,\gamma)}$ which relates the macroscopic strain tensor $\bar{\boldsymbol{\varepsilon}}$ to the microscopic strain tensor of each subcell $\bar{\boldsymbol{\varepsilon}}^{(\beta,\gamma)}$, after Equation 2

$$\bar{\boldsymbol{\varepsilon}}^{(\beta,\gamma)} = \mathbf{A}^{(\beta,\gamma)} \bar{\boldsymbol{\varepsilon}} . \tag{2}$$

The stress field within the unit cell is calculated using the constitutive relations of each subcell, while the homogenized mechanical properties of the composite material are determined using the relation

$$\mathbf{C}^* = \frac{1}{hl} \sum_{\gamma=1}^{N_\gamma} \sum_{\beta=1}^{N_\beta} h_\beta l_\gamma \mathbf{C}^{(\beta,\gamma)} \mathbf{A}^{(\beta,\gamma)}, \tag{3}$$

where h and l are the unit cell dimensions, while h_β , l_γ and $\mathbf{C}^{(\beta,\gamma)}$ are dimensions and elasticity matrix of the β,γ subcell, respectively.

3. Numerical model

The analyses in this work simulate experimental high velocity soft body impact conditions on CFRP composite plates. The experimental set-up for this analysis has been provided in (Hou, 2007). The focus of current research is application of the multiscale methodology on high velocity impact on composite structures. Therefore, the primary attention has been directed towards the validation of micromechanical failure criteria resulting from the high velocity impact loading conditions.

The numerical model is shown in Figure 2. The bird model has been modeled by the CEL formulation, which is suitable for problems in which large deformations can cause numerical difficulties for Lagrangian finite element models. In the CEL technique, the soft-body impactor is modeled as Eulerian material, which flows through the static Eulerian finite elements. Details about the CEL procedure can be found in the Abaqus Users Manual. The general contact algorithm has been used to model the complex contact conditions between the Lagrangian mesh of the composite plate and the Eulerian impactor material.

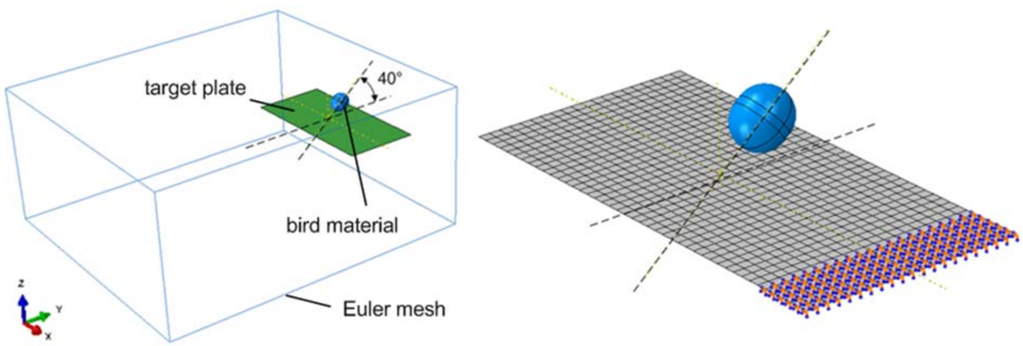

Figure 2. CEL numerical model.

The size of the cube containing Eulerian elements has to be sufficiently large to prevent the impactor material from escaping the Eulerian mesh. Therefore, the dimensions of the cube are 0.45 x 0.4 x 0.2 m, while the Eulerian model has been discretized using 487,920 elements. The impactor has been defined after (Hou, 2007) as a body with a 25 mm diameter, mass of 10 g and material density of 1010 kg/m^3. As the exact shape of the impactor has not been specified, the conventional shape used in the numerical bird strike simulations has been employed in this work. Accordingly, the substitute bird geometry has been replaced by a cylinder with hemispherical ends. The initial velocity vector is deflected by 40° with respect to the composite plate plane, as shown in Figure 2. The initial conditions have been defined by 200 m/s velocity of the bird material, as shown in Figure 2. The impact point is located at the centre of the unclamped part of the composite plate. For the simulation of the analyzed impact event, a total time of 1.2 ms has to be simulated.

A 25 mm wide clamp has been applied to one of the shorter plate edges in the experimental setup. This boundary condition has been simulated by restriction of all degrees of freedom of the nodes in the clamped part of the composite plate, as shown in the right-hand side image in Figure 2. Dimensions of the composite plate are 216 x 102 mm. The plate geometry has been discretized using 860 conventional shell finite elements. The composite plate is 3 mm thick and consists of 21 CFRP T300/914 plies with a $[(0/\,90)_5/\,\overline{0}\,]_S$ layup, where the layup angle has been measured with regard to the longer plate edge. The mechanical properties of the CFRP T300/914 unidirectional plies have in this work been predicted using the HFGMC micromechanical model, as described in Section 3.2. The homogenized properties are provided in Table 2.

The impactor material model has been modeled using the Mie-Grüneisen Equation of State which describes a linear relationship between the shock and particle velocities. This relationship has the form

$$U_S = c_0 + sU_P\,, \quad (4)$$

where U_S and U_P are shock and particle velocities, while c_0 and s are parameters which define the EOS material. The EOS properties, which have been validated in (Smojver, 2011), are c_0 = 1480 m/s (speed of sound in the material) and s = 0 (coefficient defining the linear relationship between shock and particle velocities).

3.1 Implementation of HFGMC into Abaqus/Explicit

The micromechanical model has been implemented into Abaqus/Explicit using the material user subroutine VUMAT. HFGMC is programmed as a subroutine which is called at every integration point of the explicit finite element analysis. As described in Section 1, the methodology is still in the development phase. Therefore, damage effects have not been included in the multiscale analyses of this work. The homogenized material properties and strain concentration tensors are calculated at the start of the Abaqus/Explicit analysis, based on the HFGMC solution. As the degradation of mechanical properties has been neglected, the strain concentration tensors keep the initial values. Consequently, micromechanical failure criteria can be predicted using the initial strain concentration tensors. The microscopic strain field has been calculated as a result of the macroscopic loading, after Equation 2.

Currently, three micromechanical failure criteria have been implemented, as described in Section 3.3. The maximal values of the micromechanical failure criteria are stored as solution dependent state variables (SDV) and can be visualized during post-processing. In order to further enhance the computational properties of the methodology, the current implementation uses the macroscopic Puck's criterion in order to initiate micromechanical computations. Consequently, the computationally intensive micromechanical calculations have been avoided for parts of the macroscopic finite element model which are not stressed and therefore no degradation of mechanical properties is expected. Puck's criterion has been selected for the purpose of initiation of micromechanical calculations due to its good results in the World Wide Failure Exercise (Hinton, 2004). The criterion distinguishes between fiber failure (FF) and interfiber failure (IFF - matrix failure mode). Details of Puck's failure criterion are provided in (Puck, 1998), while the mechanical properties used to calculate the criteria have been listed in Table 2, after (Puck, 2002). The micromechanical computations in this work have been initiated for integration points in which the macroscopic stress state resulted in FF or IFF criterion values above 0.1.

3.2 Micromechanical model

The two-dimensional HFGMC model has been employed in which the doubly periodic RUC is modeled with fibers oriented in the x_1 direction and arranged in a doubly periodic array in the x_2 and x_3 directions, as shown in Figure 1. The simplest unit cell morphology has been employed for analyses in this work, which consists of a single fiber in the centre of the micromechanical model. The fiber volume fraction (V_f) of the evaluated composite material is 60%. The micromechanical analyzes in this work have been performed using the RUC discretization with 40 x 40 rectangular cells as shown in the central image in Figure 3. The effect of discretization refinement on the unit cell is shown in Figure 3. Due to the traction continuity conditions at subcell boundaries, relatively coarse HFGMC models can accurately predict the stress field at the fiber/matrix boundary, after (Aboudi, 2012).

Constituent's mechanical properties, listed in Table 1, have been taken from (Soden, 1998). The homogenized mechanical properties of the T300/914 have been calculated by the HFGMC model and are listed in Table 2, along with the mechanical properties necessary for calculation of micromechanical failure criteria, as explained in Section 3.3.

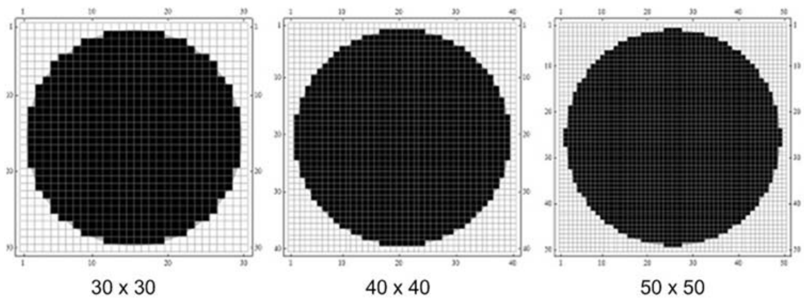

Figure 3. Unit cell discretizations.

Table 1. Constituent mechanical properties.

Fiber mechanical properties (T300 carbon fiber)				
E [GPa]	ν [-]	X_ε^T [-]	X_ε^C [-]	S_{12f} [MPa]
230	0.3	0.01086	0.00869	105
Matrix mechanical properties (914 epoxy matrix)				
E [GPa]	ν [-]	$X_\varepsilon^T = Y_\varepsilon^T = Z_\varepsilon^T$ [-]	$X_\varepsilon^C = Y_\varepsilon^C = Z_\varepsilon^C$ [-]	S_ε [-]
4	0.35	0.01875	0.03750	0.04725

Table 2. T300/914 homogenized mechanical properties and strengths, V_f= 0.6.

E_1 [GPa]	E_2 [GPa]	G_{12} [GPa]	ν_{12} [−]	ν_{23} [−]
138.473	20.344	5.869	0.314	0.257
R_{11}^t [MPa]	R_{11}^c [MPa]	R_{22}^t [MPa]	R_{22}^c [MPa]	R_{12} [MPa]
1520	1520	60	246	95
p_{12}^t [−]	p_{12}^c [−]	p_{23}^t [−]	p_{23}^c [−]	
0.3	0.35	0.27	0.23	

3.3 Micromechanical failure criteria

Three micromechanical failure initiation models have been evaluated in this work. The first failure model employs the 3D Tsai Hill criterion defined as

$$\begin{aligned}&\frac{\left(\bar{\sigma}_{11}^{(\beta,\gamma)}\right)^2+\left(\bar{\sigma}_{22}^{(\beta,\gamma)}\right)^2+\left(\bar{\sigma}_{33}^{(\beta,\gamma)}\right)^2}{Y^2}+\frac{-\bar{\sigma}_{11}^{(\beta,\gamma)}\bar{\sigma}_{22}^{(\beta,\gamma)}-\bar{\sigma}_{11}^{(\beta,\gamma)}\bar{\sigma}_{33}^{(\beta,\gamma)}-\bar{\sigma}_{22}^{(\beta,\gamma)}\bar{\sigma}_{33}^{(\beta,\gamma)}}{Y^2}+\\&+\frac{\left(\bar{\sigma}_{12}^{(\beta,\gamma)}\right)^2+\left(\bar{\sigma}_{13}^{(\beta,\gamma)}\right)^2+\left(\bar{\sigma}_{23}^{(\beta,\gamma)}\right)^2}{T^2}=d_m^2,\end{aligned} \quad (5)$$

where Y is the matrix transverse strength and T is the matrix shear strength, after (Pineda, 2009). The value of the matrix transverse strength used in Equation 5 depends on the type of the applied transverse stress

$$\begin{aligned}Y&=Y_c \quad \bar{\sigma}_{22}<0,\\ Y&=Y_t \quad \bar{\sigma}_{22}>0.\end{aligned} \quad (6)$$

Failure is initiated at stress states for which the term d_m in Equation 5 reaches values greater than 1. The maximal strain criterion has in (Pineda, 2009) been applied at fiber subcells. In this criterion, subcell strains in the fiber direction $\bar{\varepsilon}_{11}^{(\beta,\gamma)}$ are compared to the ultimate fiber strain ε_{ft}^{U},

$$\left(\frac{\bar{\varepsilon}_{11}^{(\beta,\gamma)}}{\varepsilon_{ft}^{U}}\right)^2=d_f^2. \quad (7)$$

Similarly to the matrix criterion, failure is initiated if the right-hand side term d_f in Equation 7 reaches values above 1.

The Multicontinuum Theory (MCT) defines criteria for both constituents, after (Mayes, 2004). The expressions for the theory have been derived from the quadratic interaction failure criterion, by taking into account assumptions on the failure modes for the fiber and matrix constituents, as explained in (Mayes, 2004). Contrary to the original application, the MCT failure criteria have been in this work applied to the HFGMC micromechanical model, consequently taking into account the stress variations within the unit cell instead of dealing with averaged constituent values. Failure initiation in the matrix is predicted if the stress state satisfies the relation

$$K_{3m}I_3+K_{4m}I_4=1, \quad (8)$$

where

$$K_{3m}=\frac{1}{S_{22m}^2+S_{33m}^2}, \quad (9)$$

$$K_{4m}=\frac{1}{S_{12m}^2}. \quad (10)$$

S_{12m}, S_{22m} and S_{33m} are matrix strengths in the *2* and *3* directions, which are dependent on the tensile/compressive character of the loading in the *2* direction. The MCT calculates fiber failure using the equation

$$K_{1f} I_1^2 + K_{4f} I_4 = 1\,, \quad (11)$$

where

$$K_{1f} = \frac{1}{S_{11f}^2} \quad (12)$$

and

$$K_{4f} = \frac{1}{S_{12f}^2}\,. \quad (13)$$

The S_{11f} term denotes the strength in fiber direction, which can be tensile or compressive, while S_{12f} is the fiber shear strength, which for the T300 fiber is provided in Table 2, after (Mayes, 2004). The relations in Equations 8 and 11 include the transversally isotropic stress invariants, expressed as (Mayes, 2014)

$$\begin{aligned} I_1 &= \sigma_{11}, \\ I_2 &= \sigma_{22} + \sigma_{33}, \\ I_3 &= \sigma_{22}^2 + \sigma_{33}^2 + 2\sigma_{23}^2, \\ I_4 &= \sigma_{12}^2 + \sigma_{13}^2. \end{aligned} \quad (14)$$

The third micromechanical failure theory employs the 3D Hashin-type strain based failure criterion for the matrix combined with the maximal strength criterion for the fiber, as used in (Bednarcyk, 2010). The failure criterion for the matrix subcells introduces damage strains defined as

$$\begin{aligned} \varepsilon_1^D &= \sqrt{\left(\frac{\varepsilon_{11}}{X_\varepsilon}\right)^2 + \left(\frac{\gamma_{13}}{R_\varepsilon}\right)^2 + \left(\frac{\gamma_{12}}{S_\varepsilon}\right)^2}\,, \\ \varepsilon_2^D &= \sqrt{\left(\frac{\varepsilon_{22}}{Y_\varepsilon}\right)^2 + \left(\frac{\gamma_{23}}{Q_\varepsilon}\right)^2 + \left(\frac{\gamma_{12}}{S_\varepsilon}\right)^2}\,, \\ \varepsilon_3^D &= \sqrt{\left(\frac{\varepsilon_{33}}{Z_\varepsilon}\right)^2 + \left(\frac{\gamma_{23}}{Q_\varepsilon}\right)^2 + \left(\frac{\gamma_{13}}{R_\varepsilon}\right)^2}\,, \end{aligned} \quad (15)$$

where variables X_ε, Y_ε and Z_ε are the normal failure strains while R_ε , S_ε and Q_ε are engineering shear failure strains. The three damage strains allow modeling of the multiaxial nature of failure of composite materials. Failure of matrix subcells is initiated for stress states which result in any of the three damage strains defined in Equation 15 reaching values above 1.0. Failure of fiber subcells is predicted using the maximal stress criterion, defined as

$$\frac{\bar{\sigma}_{11}^{(\beta,\gamma)}}{X^{t,c}} \geq 1, \quad (16)$$

where $X^{t,c}$ is the strength in fiber direction, while $\bar{\sigma}_{11}^{(\beta,\gamma)}$ is the micromechanical stress in the fiber direction.

4. Results

The impact event and bird material deformation is shown in Figure 4. The contours visualize the displacements in the *z* direction, which is perpendicular to the composite plate. The visualization of the EOS material motion through the Eulerian finite element mesh in Figure 4 has been achieved using the Eulerian Volume Fractions (EVF) equal to 0.6. The EVF represent the ratios by which each Eulerian element is filled with material. EVF values equal to one represent an element completely filled with material, contrary to the completely void elements which have EVF values equal to zero. The results demonstrate the ability of the numerical bird model to replicate the very high deformations of the soft-body impactor. Although simulation of approximately 0.4 ms would be sufficient to simulate the contact between the impacting material and the composite plate, simulation of next 0.8 ms was necessary to model the flexural motions of the composite plate during which high stresses have been generated.

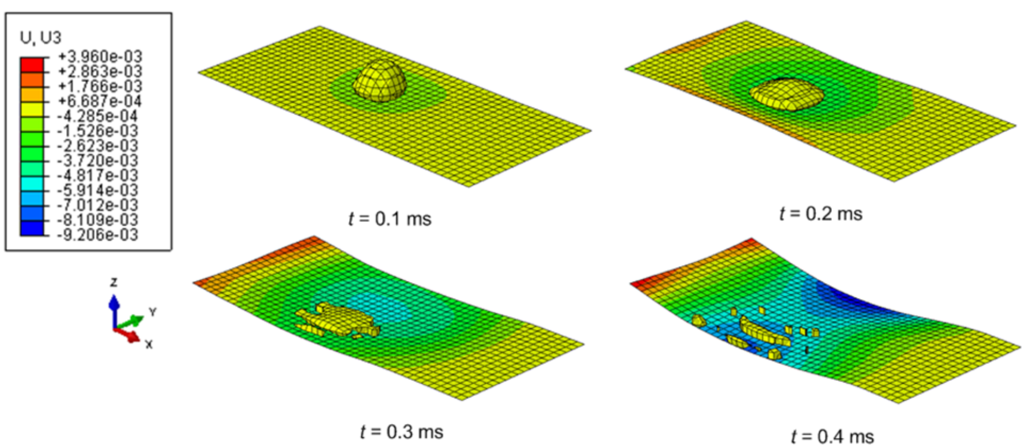

Figure 4. Visualization of the impact event. The contours show displacements in the *z* direction [m].

Comparison of the micromechanical failure criteria introduced in Section 3.3 and ply-based failure criteria has been done using the Puck failure model. Damage degradation effects on composite mechanical properties have been neglected in this work, since the introduction of damage effects to the multiscale methodology is in the focus of the ongoing research. As explained in Section 3.2, results of Puck's Mode A IFF criterion have also been used to initiate the micromechanical calculations, while the SDV's associated with micromechanical failure theories visualize maximal values of the criteria within the unit cell. Figure 5 shows comparison of the failure criteria associated with matrix failure at t = 0.1 ms. The clamped end of the composite plate is located on the right side of the images in Figures 5, 6 and 7. Although only approximately half of the impacting material has actually impacted the plate (shown by the upper left image in Figure 4), all evaluated failure criteria predict initiation of damage processes in a very large part of the composite plate.

The shapes and sizes of the failed part of the composite plate, in which failure criteria predict failure initiation, agree very well for the evaluated micromechanical matrix failure theories. However, the MCT criterion predicts initiation in the largest part of the impacted composite plate. The predicted failure surface at the considered time step (t = 0.1 ms) of the micromechanical failure criteria are slightly larger compared to the Puck's Mode A criterion.

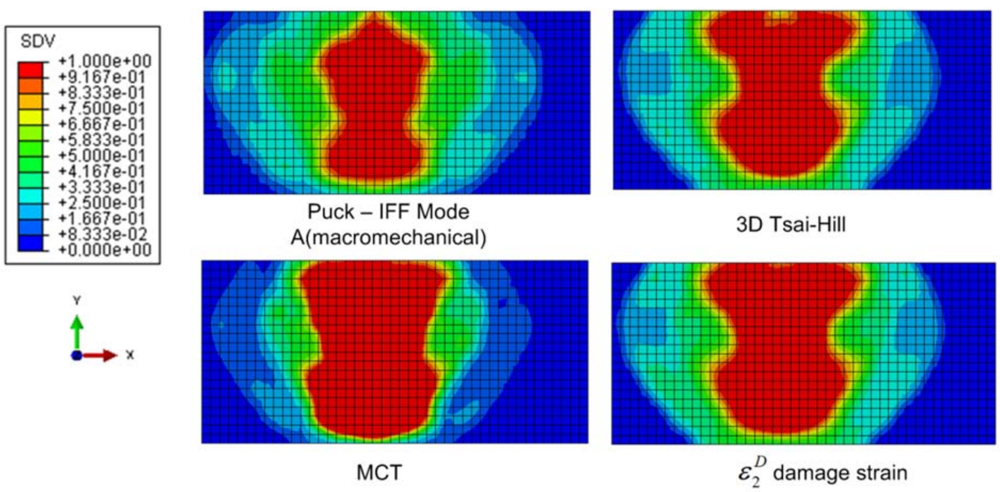

Figure 5. Comparison of the Puck IFF Mode A criterion and the micromechanical matrix failure theories (maximal through thickness values are shown at *t* = 0.1 ms).

At t = 0.1 ms, fiber failure has not been predicted by the evaluated failure criteria. The comparison of failure criteria associated with fiber failure is shown in Figure 6. As illustrated, the micromechanical maximal stress and maximal strain values contours agree very well to each other and to the macromechanical Puck's fiber tensile failure initiation contours. Analogous to the matrix failure results in Figure 5, the MCT criterion indicates the greatest values of the failure initiation criteria, which at the considered time step reaches the maximal value of 0.96.

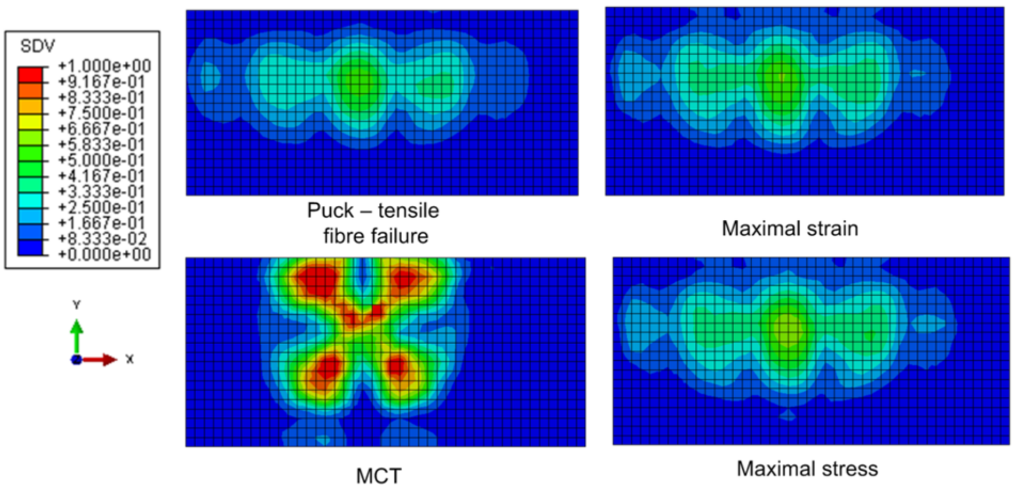

Figure 6. Comparison of the Puck tensile fiber failure and the micromechanical fiber failure theories (maximal through thickness values are shown, at *t* = 0.1 ms).

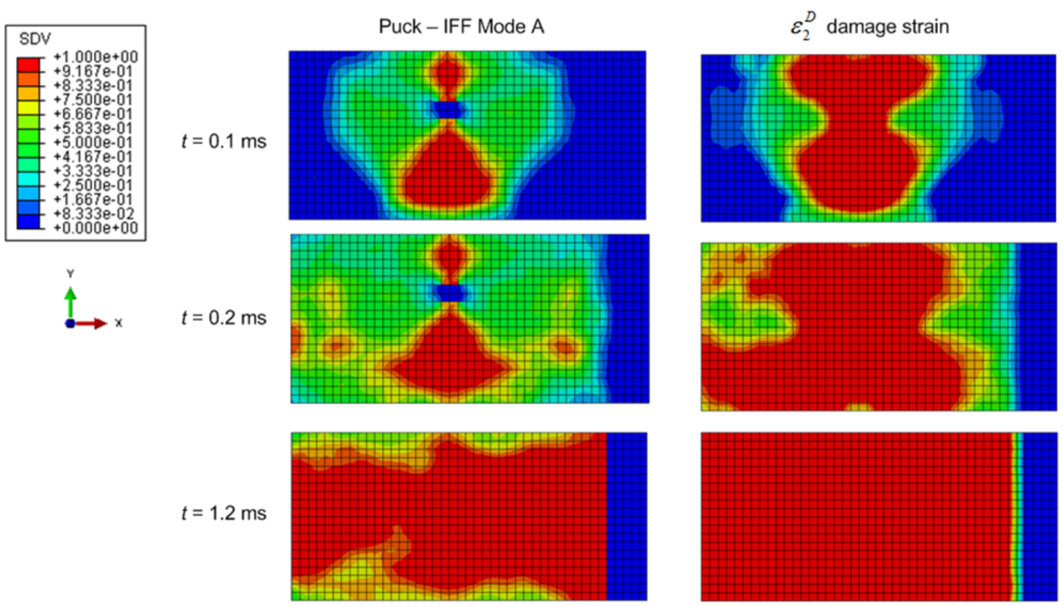

Figure 7. Evolution of Puck's Mode A IFF and the $\varepsilon_2^{\mathrm{D}}$ damage strain.

Figure 7 shows the comparison of the time dependent evolution of Puck's IFF Mode A criterion and the ε_2^D damage strain. The results in Figure 7 have been calculated at the integration points located at the composite plate side at which the soft-body impacts the plate. As illustrated, the differences between the Puck's Mode A criterion and the ε_2^D damage strain increase with the progression of the analysis. The high values of Puck's failure criterion are caused by the flexural motion of the plate at later time steps.

5. Conclusions

The analyses in this work show the results of the multiscale methodology application on a relatively complex numerical model replicating experimental high velocity soft-body impact conditions. The conclusions of the failure criteria comparison for the dynamic loading case correspond well to the conclusions obtained by the validation for static loading cases, which has been performed in (Ivančević, 2014). The MCT theory predicts for both constituents initiation of damage at the lowest loading states. A possible cause for this result is the different application of the MCT theory in the HFGMC model, as explained in Section 3.3.

Calculation of failure criteria is the first step in the numerical process of damage prediction. Micromechanical failure criteria predict onset at the subcell level and tend to be more restrictive compared to macromechanical criteria, as they generally indicate failure initiation at lower load states. The initiation of damage in one subcell does not indicate failure of the complete unit cell. For the comparison with experimental results progressive damage models have to be implemented which is in the focus of ongoing research.

The application of micromechanical models for modeling of high velocity impact problems in composite structures is particularly suitable, since such effects in composite materials affect only the matrix. The nonlinear HFGMC application (Haj-Ali, 2009) is currently being implemented into the methodology. This application will allow modeling of damage and viscoplastic effects caused by high strain rates.

6. References

1. Abaqus Users Manual, Version 6.10-1, Dassault Systémes Simulia Corp., Providence, RI.
2. Aboudi, J, A., "Closed Form Constitutive Equations for Metal Matrix Composites," International Journal of Engineering Science, vol. 25, no. 9, pp.1229-1240, 1987.
3. Aboudi, J., Arnold, S.M. and B.A. Bednarcyk, "Micromechanics of Composite Materials – a Generalized Multiscale Analysis Approach," Elsevier Science Ltd., 2013.
4. Aboudi, J., Pindera, M.-J., and S. M. Arnold, "Higher-Order Theory for Periodic Multiphase Materials with Inelastic Phases," International Journal of Plasticity, no. 19, pp. 805-847, 2003.
5. Bansal, Y., and M.-J. Pindera, "A Second Look at the Higher-Order Theory for Periodic Multiphase Materials," Journal of Applied Mechanics, no. 72, pp. 177-195, 2005.
6. Bansal, Y., and M.-J. Pindera, "Finite-Volume Direct Averaging Micromechanics of Heterogeneous Materials with Elastic-Plastic Phases," International Journal of Plasticity, no. 22, 2006.

7. Bednarcyk, B.A., Aboudi, J., and S.M. Arnold, “Micromechanics Modeling of Composites Subjected to Multiaxial Progressive Damage in the Constituents,” AIAA Journal, no. 48, 2010.
8. Haj-Ali, R., and J. Aboudi, “Nonlinear Micromechanical Formulation of the High Fidelity Generalized Method of Cells,” International Journal of Solids and Structures, no. 46, 2009.
9. Hinton, M.J., Kaddour, A.S., and P.D. Soden, “A Further Assessment of the Predictive Capabilities of Current Failure Theories for Composite Laminates: Comparison With Experimental Evidence,” Composites Science and Technology, no. 64, 2004.
10. Hou, J.P., and C. Ruiz, “Soft Body Impact on Laminated Composite Materials,” Composites: Part A, no. 38, 2007.
11. Ivančević, D., and I. Smojver, “Hybrid Approach in Bird Strike Damage Prediction on Aeronautical composite structures,” Composite Structures, no. 94, 2011.
12. Ivančević, D., and I. Smojver, “Micromechanical Damage Modelling Using a Two-Scale Method For Laminated Composite Structures,” Composite Structures, no. 108, 2014.
13. Mayes, J.S., and A.C. Hansen, “Composite Laminate Failure Analysis Using Multicontinuum Theory,” Composites Science and Technolology, no. 64, 2004.
14. Pineda, E. J., Waas, A.M., and B. A. Bednarcyk, “Multiscale Model for Progressive Damage and Failure of Laminated Composites Using an Explicit Finite Element Method,” 50th AIAA/ASME/ASCE/AHS/ASC Structures, Structural Dynamics, and Materials Conference, 2009.
15. Puck, A., and H. Schürmann, “Failure Analysis of FRP Laminates by Means of Physically Based Phenomenological Models,” Composites Science and Technology, no. 58, 1998.
16. Puck, A., Kopp, J., and M. Knops, “Guidelines for the Determination of the Parameters in Puck’s Action Plane Strength Criterion,” Composites Science and Technology, no. 62, 2002.
17. Smojver, I., and D. Ivančević, “Bird Strike Damage Analysis in Aircraft Structures Using Abaqus/Explicit and Coupled Eulerian Lagrangian Approach,” Composites Science and Technology no. 71, 2011.
18. Smojver, I., and D. Ivančević, “Advanced Modelling of Bird Strike on High Lift Devices Using Hybrid Eulerian–Lagrangian Formulation,” Aerospace Science and Technology, no. 23, 2012.
19. Soden, P.D., Hinton, M.J., and A.S. Kaddour, “Lamina Properties, Lay-up Configurations and Loading Conditions for a Range of Fibre-Reinforced Composite Laminates,” Composites Science and Technology, no. 58, 1998.